Lithium Batteries

DOI: 10.1002/ange.200907319

Dynamic Visualization of the Electric Potential in an All-Solid-State Rechargeable Lithium Battery**

Kazuo Yamamoto, Yasutoshi Iriyama,* Toru Asaka, Tsukasa Hirayama, Hideki Fujita, Craig A. J. Fisher, Katsumasa Nonaka, Yuji Sugita, and Zempachi Ogumi*

Rechargeable batteries[1] are increasingly viewed as an important means of alleviating problems associated with an overdependence on fossil fuels, as they can serve as storage devices for renewable energy, such as wind and solar power, and as power sources in environmentally friendly vehicles (fully electric and hybrid cars).[2] Of the several battery technologies available, lithium ion batteries (LIBs) are considered the most promising because they provide the largest energy storage densities.[3] However, conventional LIBs have problems that limit their scalability, particularly in regard to safety, lifetime, cost, and power density. All-solid-state LIBs containing nonflammable solid electrolytes offer the possibility of avoiding some of the safety issues associated with conventional LIBs containing combustible liquid electrolytes. Moreover, all-solid-state LIBs have increased cycle life and energy density,[4] and in principle can be manufactured more cheaply because they do not require air-tight packaging or state-of-charge monitoring circuits. The chief problem of all-solid-state LIBs is their lower power density, and this is mostly attributed to the large resistance to lithium ion transfer across the positive-electrode/solid-electrolyte interface.[5]

Despite extensive efforts to analyze reaction mechanisms for a number of different component materials and LIB chemistries,[5,6] to date it has not been possible to visualize the electric potential distribution across working devices at the nanometer scale. Dynamic observation of the potential profile and its distribution across the electrode/electrolyte interface in particular would help identify sources of resistance, enabling more efficient and robust batteries to be developed through a combination of nanoengineering and materials design. With this objective, we used quantitative electron holography (EH)[7] to directly observe the potential distribution resulting from lithium-ion diffusion in all-solid-state LIBs operated within a transmission electron microscope (TEM). The results reveal in unprecedented detail how the potential due to lithium ions is distributed across a $LiCoO_2$ positive-electrode/solid-electrolyte interface during charge–discharge reactions. A steep potential drop and a gradually extended slope owing to the electrical double layer are formed near the interface, where the resistance to lithium ion transfer occurs.

To directly observe the battery reaction occurring near the electrode/electrolyte interface in a TEM, a planar all-solid-state LIB was prepared in the configuration shown in Figure 1 a. A 90 μm thick glass ceramic sheet of composition $Li_{1+x+y}Al_yTi_{2-y}Si_xP_{3-x}O_{12}$ (ionic conductivity $\sigma = 10^{-4}$ S cm^{-1} at room temperature; OHARA Inc., Japan) was used as the solid electrolyte.[8] A positive electrode of crystalline $LiCoO_2$ was deposited on one side of the sheet by pulsed laser deposition (PLD) to a thickness of 800 nm, and a gold film was then deposited on top to act as a current collector.[9] The other side was coated with platinum, and the negative electrode was prepared by partial decomposition of the electrolyte sheet near the platinum current collector.[10]

The red box in Figure 1 a indicates the region thinned for TEM observation by a 40 kV focused ion beam (FIB), using gallium ions, to a thickness of about 60 nm. The battery was loaded on a specially designed TEM holder equipped with two fixed electrodes for applying voltage. Figure 1 b shows the initial cyclic voltammogram (CV) obtained in the TEM. The voltage was swept to 2.0 V at 40 mV min^{-1}. Symmetrical anodic and cathodic current peaks can be assigned to the electrochemical movement of lithium ions from the positive to the negative electrode, and the reverse process, respectively. In the positive electrode, $LiCoO_2$, the largest amount of lithium insertion/extraction occurs at 3.93 V (vs. Li/Li$^+$),[11] whilst for the negative electrode it is at 2.35 V (vs. Li/Li$^+$).[10] Therefore, the peak voltage of around 1.6 V in Figure 1 b is consistent with the difference between the potentials of the two electrodes.

Figure 2 a shows a bright-field TEM image of the positive-electrode/electrolyte interface. The electrode has a columnar microstructure orientated perpendicular to the electrolyte

[*] Dr. K. Yamamoto, Dr. T. Asaka, Dr. T. Hirayama, Dr. H. Fujita, Dr. C. A. J. Fisher
Nanostructures Research Laboratory, Japan Fine Ceramics Center
2-4-1 Mutsuno, Atsuta-ku, Nagoya, 456-8587 (Japan)
Fax: (+81) 52-871-3500
E-mail: k-yamamoto@jfcc.or.jp
Prof. Dr. Y. Iriyama
Department of Materials Science and Chemical Engineering
Faculty of Engineering, Shizuoka University
3-5-1 Johoku, Naka-ku, Hamamatsu, Shizuoka, 432-8561 (Japan)
Fax: (+81) 53-478-1168
E-mail: tyiriya@ipc.shizuoka.ac.jp
K. Nonaka, Dr. Y. Sugita
Chubu Electric Power Co., Inc.
20-1 Kitasekiyama, Ohdaka-cho
Midori-ku, Nagoya, 459-8522 (Japan)
Prof. Dr. Z. Ogumi
Innovative Collaboration Center, Kyoto University
Nishikyo-ku, Kyoto, 615-8520 (Japan)

[**] This work was financially supported by Chubu Electric Power Co., Inc. We thank Dr. H. Moriwake, Dr. A. Kuwabara and Dr. R. Huang for valuable discussions. We are grateful to OHARA Inc. for supplying the glass ceramic sheet used as the solid electrolyte.

Supporting information for this article is available on the WWW under http://dx.doi.org/10.1002/anie.200907319.

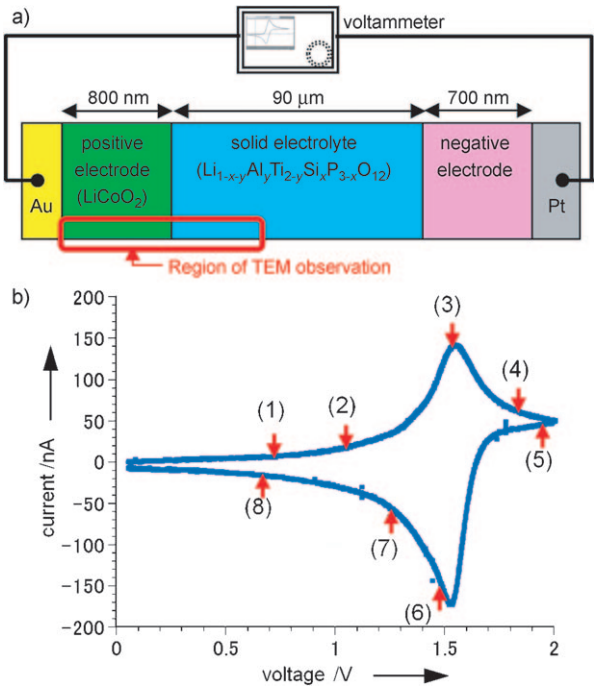

Figure 1. a) The all-solid-state LIB sample. The red-boxed region was thinned by a focused ion beam and observed by electron holography. b) Cyclic voltammogram measured in a TEM with a voltage sweep rate of 40 mV min^{-1}. EH images were taken at points (1)–(8), and are given in Figure 2 b–i, respectively.

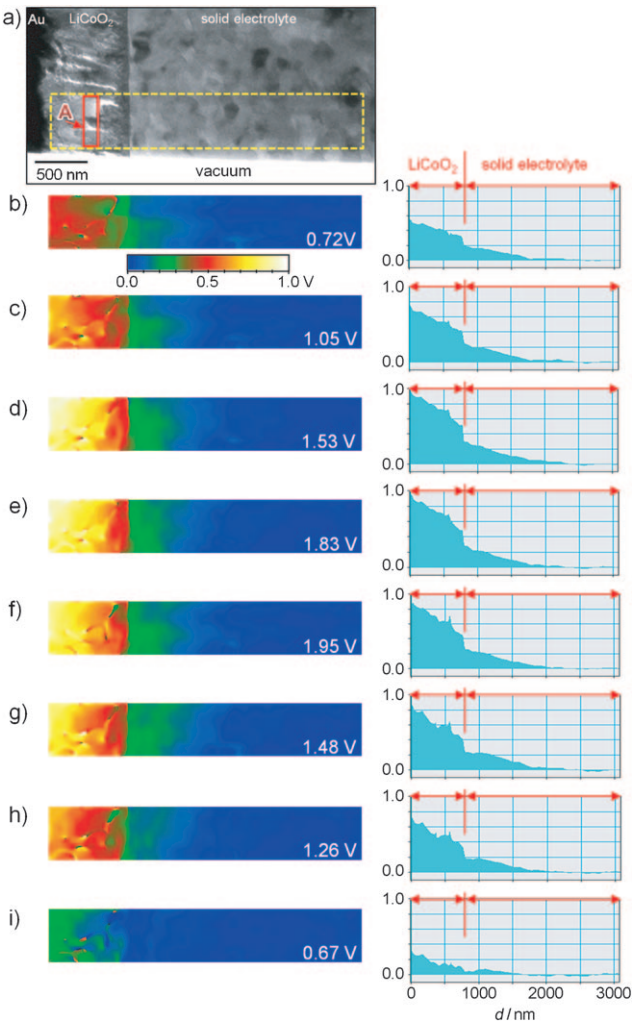

Figure 2. Electric potential distribution around the $LiCoO_2$/electrolyte interface during the charge–discharge process. a) Bright-field TEM image of the region near the interface. b–i) 2D potential images (left) and line profiles (right) for the region bounded by the dashed line in Figure 2 a and obtained at voltages corresponding to points (1)–(8) in Figure 1 b. Potential [V] is given on the *y* axis.

sheet. Electron interference fringe patterns, or "holograms", were obtained for the region enclosed by the yellow dashed line in Figure 2 a at different applied voltages corresponding to labels (1)–(8) in the CV of Figure 1 b. The corresponding potential images and line profiles perpendicular to the interface were then extracted (Figure 2 b–i). Extraneous potential signals resulting from variations in sample thickness and electron charging were removed by subtracting the potential for the initial state (0 V) from that in the applied state. Some noise is apparent in the $LiCoO_2$ region, which is caused by electron diffraction that perturbs the contrast and spacing of the electron interference fringes in the holograms.

The line profiles clearly show that the electric potential height of the positive electrode varies gradually with the applied voltage. In contrast, far from the interface the potential in the electrolyte did not change at all, regardless of the voltage. This result indicates that the resistance is mainly concentrated near the interface, which is consistent with the generally accepted model of potential distribution at an interface.[12] Although the overall battery voltage is the net difference in potential between positive and negative electrodes, the profiles reveal how the potential is distributed internally, providing critical information on the different components and their interactions. Several characteristic features are discernible in these potential profile curves; for example, in $LiCoO_2$, the profile has a relatively linear slope, with a steep potential drop at the interface, and a gradual slope in the solid electrolyte near the interface. These characteristic profiles were completely reversible during repeated charge–discharge cycles and disappeared when the voltage was removed.

To verify that changes in the potential profile were due to lithium ion movement, electron energy loss spectroscopy (EELS) analysis was performed. The average change in valence of cobalt ions in $LiCoO_2$ upon lithium extraction was measured from the EELS spectra of cobalt taken in the cross-section "A" in Figure 2 a. Figure 3 shows the core-loss spectra for the Co L-edge in uncharged (0 V) and charged (1.6 V) states. During charging, the energy-loss peak increased by 0.4 eV, indicating an increase in the average valence number of cobalt.[13] In contrast, the zero-loss EELS peak did not shift during the period of exposure (18 s). These results confirm that cobalt was partially oxidized from Co^{3+} to Co^{4+} during charging as a result of removal of lithium ions from $LiCoO_2$.

Figure 4 a shows the lithium ion and electron distributions near the positive-electrode/electrolyte interface during charging, and typical distribution of the measured potential. When

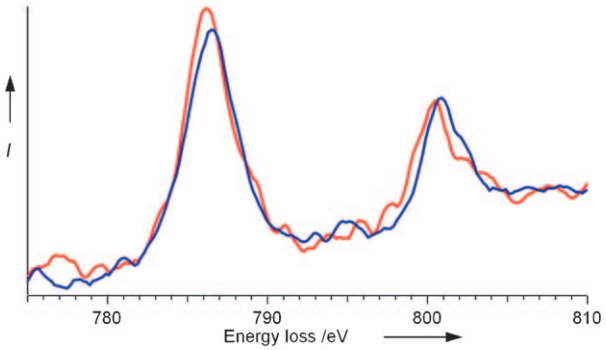

Figure 3. Co L-edge electron energy loss spectra from the $LiCoO_2$ material in uncharged (red) and charged states (1.6 V; blue). Both spectra were obtained from cross-section "A" in Figure 2a.

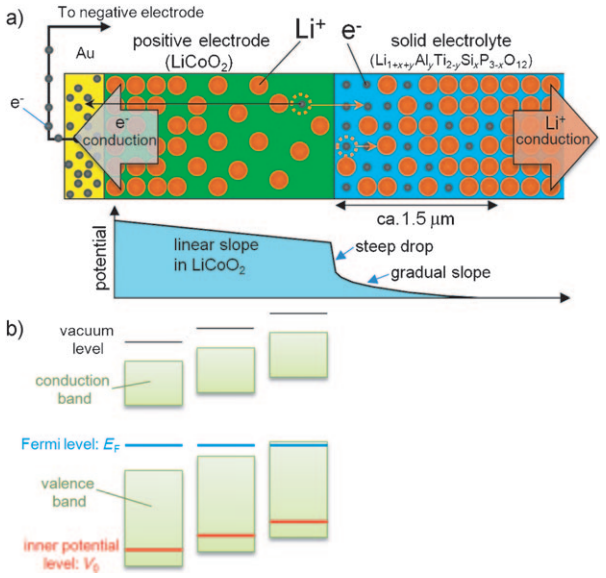

Figure 4. Effect of lithium extraction on $LiCoO_2$ band structure and the concomitant formation of an electric double layer. a) Lithium and electron distributions near the positive-electrode/electrolyte interface in the charged state (top), and typical distribution of the measured potential (bottom). b) Extraction of lithium ions from $LiCoO_2$ leads to a shift of the electronic band structures. The resulting shift of the inner potential level V_0, as measured by electron holography, is manifested in the slopes of the potential plots in Figure 2b–i. An electric double layer forms at the interface as a result of lithium ion diffusion, leading to the observed potential drop at the interface and the gradual slope of the potential in the electrolyte (Figure 2b–i).

lithium ions are extracted from $LiCoO_2$ via the interface, oxidation of the positive electrode material occurs to maintain charge balance, as evident from the EELS spectra (Figure 3). Consequently, holes form in the valence band and the Fermi level decreases,[14] as illustrated in the band structure diagrams (Figure 4b), resulting in enhanced electronic conductivity.[15] The inner potential level V_0 measured by EH is roughly defined as the volume average of the atomic electrostatic potential owing to positively charged nuclei and negatively charged electrons.[16] Therefore, its position in the valence band does not change significantly during charge–discharge cycles because lithium is a much lighter element than the others in the system (cobalt and oxygen). Moreover, the average amount of extracted lithium is assumed to be less than 50%, as no characteristic peaks corresponding to the hexagonal–monoclinic structural phase transition of $LiCoO_2$ were observed in the CV.[11] When the band structures shift such that the Fermi levels in the $LiCoO_2$ align, the local differences in V_0 become apparent. These differences can be detected by EH, producing the linear potential slopes in the $LiCoO_2$ region. Stated simply, the slope of the potential curve in the $LiCoO_2$ represents local differences in lithium ion concentration. Note that the sign of the vertical axes in Figure 2b–i is positive, which is opposite to that for electronic band structures (Figure 4b).

The potential profiles in Figure 2b–i drop steeply at the interface, and then gradually decrease over a distance of 1.5 µm in the electrolyte. In general, when a positive potential is applied to an electrode, a negatively charged region forms on the electrolyte side of the interface. In our case, the solid electrolyte permits rapid movement of positively charged lithium ions, but not the host ions (aluminum, titanium, silicon, phosphorus, and oxygen), whilst electrons also have a low diffusion rate and thus cannot move as fast as the lithium ions. Lithium ions in the electrolyte thus move away from the interface and towards the negative electrode, forming a lithium-poor region with net negative charge according to the reaction:

$$Li_{1+x+y}Al_yTi_{2-y}Si_xP_{3-x}O_{12} \rightleftharpoons (Li_{1+x+y-z}Al_yTi_{2-y}Si_xP_{3-x}O_{12})^{z-} + z\,Li^+$$

The thickness of this space charge or electrical double layer constitutes a measure of the Debye length, which can generally be estimated using the Poisson–Boltzmann equation in accordance with the Gouy–Chapmann theory.[17] The estimate of the Debye length obtained using the lithium concentration in the solid electrolyte is on the order of a few Ångströms only, which is much shorter than that observed in the profiles (ca. 1.5 µm). However, the theoretical model only takes into account electrostatic interactions between uniform charges formed on the electrode surface and the mobile ions, and neglects other interactions. The holographic results thus indicate that lithium ions in the solid electrolyte are subject to other interactions, as is the case in concentrated liquid electrolytes. Thermodynamic analysis of the potential profiles should enable the formation mechanism of the charge region in the electrolyte to be elucidated. This analysis is currently in progress.

In conclusion, we have succeeded in directly observing changes of electric potential in an all-solid-state LIB during charge–discharge cycles. EH has been used to successfully quantify the 2D potential distribution resulting from movement of lithium ions near the positive-electrode/electrolyte interface. This result was confirmed using EELS results, which showed that lithium extraction from the positive electrode during charging results in oxidation of cobalt from Co^{3+} to Co^{4+}. Quantitative analysis of these data will allow the sources of reaction resistance in all-solid-state batteries to be identified, and particularly kinetic factors controlling charge–discharge reactions at the interface. This in-situ observation

technique based upon quantitative EH combined with EELS promises to be a powerful technique for characterizing not only LIBs but also electric double layer capacitors, fuel cell batteries, and other electrochemical devices.

Experimental Section

An 800 nm thick film of $LiCoO_2$ was deposited at 873 K for 10 h on the solid electrolyte (OHARA Inc.) by PLD.[9] When the Au/$LiCoO_2$/solid-electrolyte/Pt cell was first charged, with the $LiCoO_2$ side positive, excess lithium ions accumulated at the electrolyte/Pt interface. As a result, partial and irreversible decomposition of the electrolyte occurred near the interface, with the resultant phase serving as the negative electrode.[10] EH and EELS were performed with a 300 kV EH TEM and a 200 kV aberration-corrected TEM, respectively. The details of our TEM holder and EH analysis are described in Supporting Information.

Received: December 29, 2009
Published online: May 12, 2010

Keywords: electrochemistry · electron holography · electron microscopy · lithium batteries · solid-state reactions

[1] M. Armand, J.-M. Tarascon, *Nature* **2008**, *451*, 652 – 657.
[2] a) C. C. Chan, K. T. Chau, *Modern Electric Vehicle Technology*, Oxford University Press, New York, **2001**; b) J. Tollefson, *Nature* **2008**, *456*, 436 – 440.
[3] J.-M. Tarascon, M. Armand, *Nature* **2001**, *414*, 359 – 367.
[4] J. B. Bates, N. J. Dudney, B. Neudecker, A. Ueda, C. D. Evans, *Solid State Ionics* **2000**, *135*, 33 – 45.
[5] N. Ohta, K. Takada, L. Q. Zhang, R. Z. Ma, M. Osada, T. Sasaki, *Adv. Mater.* **2006**, *18*, 2226 – 2229.
[6] a) F. Croce, G. B. Appetecchi, L. Persi, B. Scrosati, *Nature* **1998**, *394*, 456 – 458; b) P. S. Herle, B. Ellis, N. Coombs, L. F. Nazar, *Nat. Mater.* **2004**, *3*, 147 – 152; c) T. Abe, F. Sagane, M. Ohtsuka, Y. Iriyama, Z. Ogumi, *J. Electrochem. Soc.* **2005**, *152*, A2151 – A2154; d) J. Maier, *Nat. Mater.* **2005**, *4*, 805 – 815; e) T. Ogasawara, A. Debart, M. Holzapfel, P. Novak, P. G. Bruce, *J. Am. Chem. Soc.* **2006**, *128*, 1390 – 1393; f) C. Delmas, M. Maccario, L. Croguennec, F. Le Cras, F. Weill, *Nat. Mater.* **2008**, *7*, 665 – 671; g) A. Brazier, L. Dupont, L. Dantras-Laffont, N. Kuwata, J. Kawamura, J. M. Tarascon, *Chem. Mater.* **2008**, *20*, 2352 – 2359.
[7] a) D. Gabor, *Nature* **1948**, *161*, 777 – 778; b) A. Tonomura, *Electron Holography*, *Springer Series in Optical Sciences*, *Vol. 70*, Springer, Heidelberg, **1999**.
[8] J. Fu, *J. Am. Ceram. Soc.* **1997**, *80*, 1901 – 1903.
[9] Y. Iriyama, M. Inaba, T. Abe, Z. Ogumi, *J. Power Sources* **2001**, *94*, 175 – 182.
[10] Y. Iriyama, C. Yada, T. Abe, Z. Ogumi, K. Kikuchi, *Electrochem. Commun.* **2006**, *8*, 1287 – 1291.
[11] J. N. Reimers, J. R. Dahn, *J. Electrochem. Soc.* **1992**, *139*, 2091 – 2097.
[12] J. O'M. Bockris, A. K. N. Reddy, *Modern Electrochemistry*, Plenum, New York, **1970**.
[13] a) O. L. Krivanek, J. H. Paterson, *Ultramicroscopy* **1990**, *32*, 313 – 318; b) J. H. Paterson, O. L. Krivanek, *Ultramicroscopy* **1990**, *32*, 319 – 325.
[14] J. B. Goodenough in *Oxide Cathodes* (Eds.: W. A. Schalkwijk, B. Scrosati), Kluwer/Plenum, New York, **2002**, pp. 135 – 154.
[15] a) M. Menetrier, I. Saadoune, S. Levasseur, C. Delmas, *J. Mater. Chem.* **1999**, *9*, 1135 – 1140; b) G. Ceder, A. Van der Ven, *Electrochim. Acta* **1999**, *45*, 131 – 150.
[16] M. Gajdardziska-Josifovska, A. H. Carim in *Introduction to Electron Holography* (Eds.: E. Völkl, L. F. Allard, D. C. Joy), Kluwer/Plenum, New York, **1999**, pp. 267 – 293.
[17] J. Maier, *Physical Chemistry of Ionic Materials: Ions and Electrons in Solids*, Wiley, Chichester, **2005**.

